Mon. Not. R. astr. Soc. (1980) **191**, 615–630 and *Microfiche* MN191/1

Neutral hydrogen in IC 342 – II. The detailed structure

K. Newton *Mullard Radio Astronomy Observatory, Cavendish Laboratory, Madingley Road, Cambridge CB3 0HE*

Received 1979 October 2

Summary. H I in the Scd galaxy IC342 has been studied with a resolution in radial velocity of 16 km s^{-1} and with an angular resolution (1.9 × 2.0 arcmin) sufficient to resolve detailed spiral structure. Spiral arms extend over the outer, warped parts of the disc, and reach the limit of detected H I at ~ 40 arcmin (50 kpc) from the nucleus. The pattern is multi-armed, with the clearest features lying beyond the observed optical emission, and inner arms which are well correlated with other Population I material. If the arms are quasi-stationary density-wave features, the absence of radial streaming motions > 5 km s^{-1} implies a small pattern speed. A marginal detection of such motions along one arm is consistent both with this result and with the conclusion derived from the H I distribution that corotation is between 16 and 21 kpc from the nucleus, and the pattern speed is ~ 10 km s^{-1} kpc^{-1}.

1 Introduction

An aperture synthesis survey of H I in the Scd galaxy IC342 has been made with the Cambridge Half-Mile telescope (Newton 1980b, Paper I). Details of the observations and methods of data reduction were discussed in Paper I, together with the large-scale structure of the galaxy. A low-brightness extension to the north-west of the main H I distribution was detected as far as 43 arcmin from the nucleus, and perturbations in the radial-velocity field were interpreted as warping of the plane in the outer regions.

The present paper examines the detailed structure by means of maps with an angular resolution of 1.9 × 2.0 arcmin, sufficient to resolve clear spiral structure. The maps are presented in Section 2 and the spiral structure is described in Section 3. A comparison with the distribution of other Population I material is given in Section 4. Velocity dispersions of the H I gas are investigated in Section 5, and the radial-velocity field and its relation to the spiral structure is discussed in Section 6.

1 arcmin = 1.31 kpc; values of systemic velocity = 25 km s^{-1}, inclination = 25° and p.a. of the major axis = 39° are assumed for the central disc. All radial velocities are heliocentric and map coordinates are for epoch 1950.0.

2 Details of the high-resolution maps

Spectral observations provided 32 output maps with separations of 13.2 km s^{-1} in radial velocity, each representing a velocity range of 16 km s^{-1}. The maps with angular resolution 1.9 x 2.0 arcmin are presented in Appendix 1 (*Microfiche* MN 191/1), and details of the survey are summarized in Table 1. Confusion by emission from H I in our Galaxy over the velocity range -2 to -68 km s^{-1} is considerably reduced in comparison with the low-resolution maps (Paper I) on account of the lesser sensitivity of the high-resolution maps to extended features of low brightness. Nevertheless, the correction procedures described in Paper I were applied to the data in order to produce maps with minimum contamination from the local H I and corrected for absorption effects. The resulting velocity profiles are generally simple and single-peaked, with the exception of some areas where a few profiles have low-brightness secondary peaks at -15 km s^{-1}. These subsidiary features are due to residual local H I emission, and are excluded from the maps of integrated H I and radial velocity by the reduction procedure which fits only a single component to the data.

2.1 THE MAPS

Fine structure is visible on the high-resolution output maps (Appendix 1), with concentrations of emission having typical peak brightness temperatures of ~ 20 K, reaching 25 K on some maps; emission from the 'north-west extension' also shows fine structure with emission peaks reaching ~ 12 K. The H I optical depth is assumed to be small in the following discussion.

Fig. 1 shows the map of integrated H I emission ($\int T_b\, dv$, where T_b is the brightness temperature and the integration is over a radial velocity range of -81.2 to $+129.8$ km s^{-1}). The map contains a mass of H I ~ 87 per cent of that measured from the map at 7.0 x 7.6 arcmin (Paper I). The difference is due mainly to the absence from Fig. 1 of extended emission with brightness comparable to the noise level. The difference between the zero-levels of the two maps is small. The (small) errors introduced by the integration procedure are discussed by Newton (1980a).

Table 1. Details of the observations.

Field centre (1950.0)	RA $03^h\,41^m\,58^s$ DEC 67° 56′ 27″		
Mean epoch of survey	1975.1		
Number of spacings observed	48		
Spacing interval	6.1 m		
Smallest spacing	12.2 m		
Largest spacing	298.7 m		
Angular diameter of first grating response	2°		
Primary beam FWHP	94 arcmin		
Angular structure absent	$\gtrsim 1°$		
System noise temperature	120 K		
Hydrogen line receiver			
centre frequency	1420.4 MHz		
bandwidth	2 MHz		
velocity channel separation	13.2 km s^{-1}		
velocity resolution	16 km s^{-1}		
Number of spacings included	12	24	48
Angular resolution (arcmin)	7.0 x 7.6	3.6 x 3.9	1.9 x 2.0
Rms noise level over 16 km s^{-1} velocity range (K)	0.13	0.36	1.20

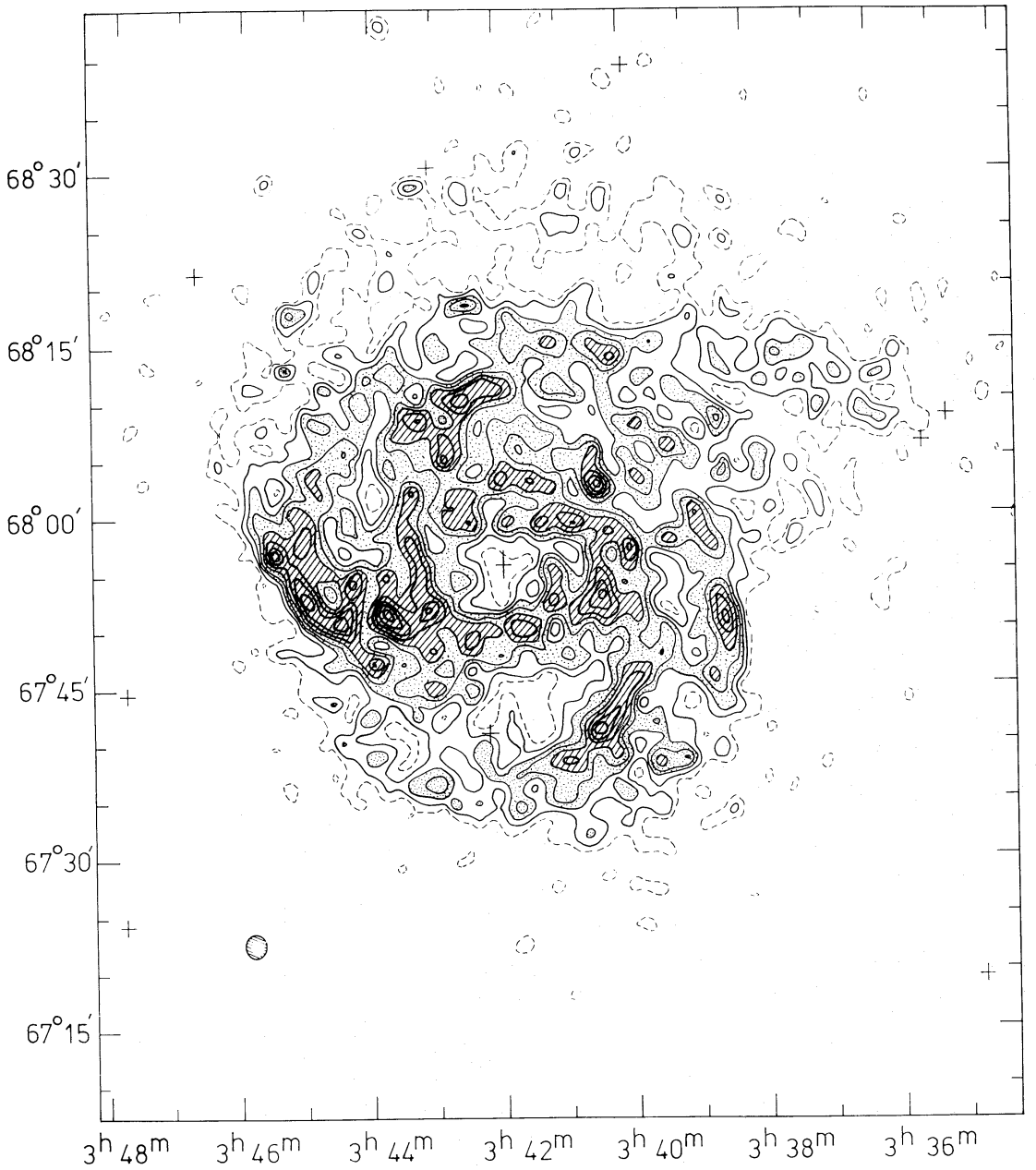

Figure 1. Contour map of the integrated H I emission from IC342 at 1.9 × 2.0 arcmin resolution. This map, and the following maps of integrated emission, have been corrected for the primary beam response. The contour interval is 100 K km s^{-1} (= 1.8 × 10^{20} atom cm^{-2} on the assumption of small optical depth) and the first contour, shown dashed, is at 100 K km s^{-1}. The rms noise level is 35 K km s^{-1} at the map centre, which is marked by the large cross. The synthesized beamshape (FWHP) is indicated by the shaded ellipse and the positions of bright foreground stars are shown by small crosses.

Detailed structure is more clearly visible on the photographic representation shown in Plate 1. The emission may be conveniently divided into the following regions.

(i) The central region: the depletion of H I around the nucleus has an irregular outline, ~ 5 arcmin (6.5 kpc) across, with an extension to the west reaching 7 arcmin from the nucleus. Emission falls below the lowest contour (100 K km s^{-1}) towards the centre. This may underestimate true values because the large velocity gradient in the region could result in broad profiles with low brightness. Output maps at 3.6 × 3.9 arcmin resolution (Paper I),

which are more sensitive to low-brightness emission while still able to resolve the 'hole', provide a 3σ upper limit of $\int T_b\,dv \leqslant 150\,\mathrm{K\,km\,s^{-1}}$. The parameters of this central depletion are in good agreement with values for similar features found in other Scd galaxies.

(ii) A region coincident with the optical emission ($5 < R < 15$ arcmin): H I emission from this region is irregular and contains features with average integrated brightness temperatures of $\sim 500\,\mathrm{K\,km\,s^{-1}}$. Several spiral segments are visible and are compared with optical emission in Section 4.

(iii) A region containing bright H I spiral structure beyond the optical arms ($15 < R < 25$ arcmin): the H I distribution shows very clear spiral structure, having the brightest emission peaks on the map (700–$900\,\mathrm{K\,km\,s^{-1}}$). The best-defined features lie beyond the optical spiral structure and are well separated even by the 2.5-kpc beam. The arms are irregular on a scale of a few kpc, with many unresolved concentrations.

(iv) The remainder of the emission ($R > 25$ arcmin): the true nature of the north-west extension is now more apparent; the entire region contains well-defined spiral features extending close to the limit of H I detected on the low-resolution maps (~ 50 kpc; Paper I). The arms again show a broken structure with emission peaks typically 200–$300\,\mathrm{K\,km\,s^{-1}}$. Patchy emission to the north of Fig. 1 is part of a low-brightness spiral feature extending from the east to the north-west and reaching 36 arcmin (47 kpc) from the nucleus. The continuity of this feature, and others in the outer parts of IC342, may be seen more clearly on the map at 3.6×3.9 arcmin resolution shown in Plate 2. Much of the observed H I in this region is contained in the spiral arms. Integration of emission in the north-west extension from Fig. 1 gives a value 54 per cent of that obtained from the map at 7.0×7.6 arcmin resolution shown in Paper I. The overall fraction of detected emission contained in the spiral features is therefore ≈ 30 per cent.

2.2 THE RADIAL H I DISTRIBUTION

Integration of Fig. 1, in circular rings in the plane of the galaxy, gives the mean radial distribution of H I shown in Fig. 2. The peak at $R = 9$ arcmin (11.8 kpc) corresponds to a ring-like structure similar to that seen in M31 but not so prominent. Roberts (1967), from

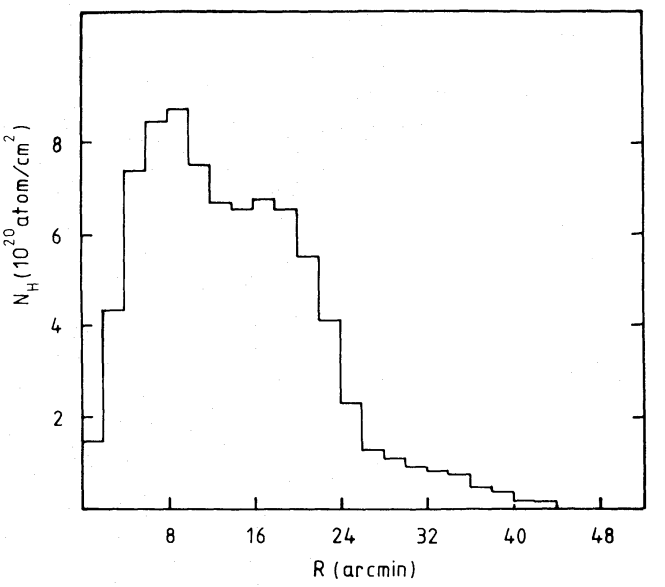

Figure 2. Radial distribution of H I in IC342 obtained by integration of Fig. 1 in circular rings in the plane of the galaxy, assuming p.a. of the major axis = 39° and disc inclination = 25°.

observations with 10 arcmin resolution, suggested the presence of an H I ring in IC342 with radius 17 arcmin and width 5.3 arcmin. Fig. 1 shows that some of the *brightest* H I features lie in this region, but the *average* surface density is approximately constant for $12 < R < 20$ arcmin, with a value of 6.0×10^{20} H atom cm^{-2} projected normal to the plane.

Beyond $R = 20$ arcmin, the surface density falls off very rapidly to 2.2×10^{20} atom cm^{-2} at $R = 25$ arcmin. This is due largely to the steep gradient of emission in the south. Similar features in M33 have been explained by Rogstad, Wright & Lockhart (1976) as projection effects caused by severe warping of the plane. This is unlikely to be the explanation here; if the model presented in Paper I is a good indication of the magnitude of a warp in IC342, no such sharp cut-off is expected. The 'shoulder' in Fig. 2 for $R > 25$ arcmin is due mainly to emission from the north-west extension.

3 Spiral structure

In view of the 2.5-kpc resolution of the present survey, a surprisingly high fraction of the H I gas shown on Plate 1 is contained in large-scale spiral features. In many galaxies, spiral structure would not be resolved at this scale. Fig. 3 shows a sketch of prominent spiral features, numbered for ease of reference. Although Plate 1 presents a clear spiral appearance to the eye, there is no unambiguous and symmetrical spiral pattern; the spiral structure is multi-armed and the arms branch at several points. There are spiral segments within the inner region ($R < 12$ arcmin), typically 10 arcmin (13 kpc) in length, of which arm 9 is the best defined. This arm is well marked by other spiral tracers and is discussed in Section 4. The outer arms extend over very long distances, typically 30 arcmin (40 kpc).

The spiral features are well separated and often have large ratios in projected density between arm and interarm regions. Arms 1 and 2 in the outer region are particularly well-separated and have average arm–interarm contrast ratios of 3.3:1 but with considerable small-scale variations. Arm 9 in the inner region, where features are not so well separated,

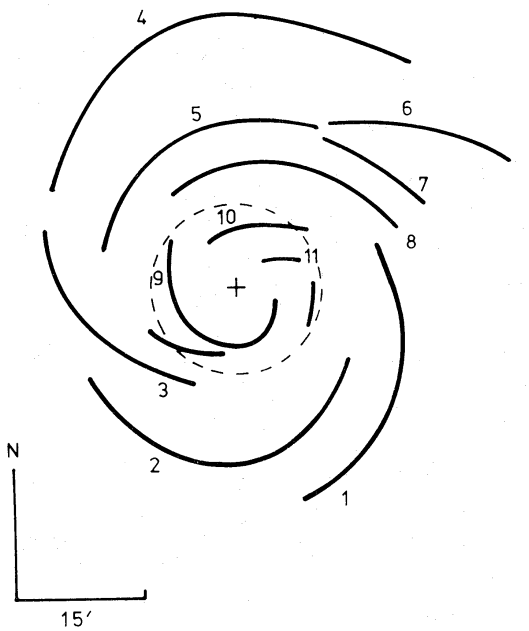

Figure 3. Sketch indicating prominent spiral features in the distribution of integrated H I emission from IC342 shown in Plate 1. The approximate extent of the 'easily visible' optical spiral structure is indicated by the dashed circle.

has an average contrast ratio of 1.7:1. Difficulties in the calculation of contrast ratios are summarized by Newton (1980a), but it should be noted that the true values could be larger than these, since H I may be optically thick in dense concentrations, and the compression region of the gas in unresolved spiral features may be on a still smaller scale than observed here. In M81, M33 and M31, for example, H I spiral features are often unresolved at the resolutions of ~ 200 pc achieved by recent observations (Rots & Shane 1975; Newton 1980a; Unwin 1980). The contrast ratios observed for IC342 should therefore be considered as lower limits.

A fit of logarithmic spiral curves to the best-defined arms gives a pitch angle, t, close to 9° for most features, and this value will be adopted for further discussion. There are two significant exceptions: arm 3, close to the south-east minor axis, has $t \simeq 12°$, but arm 4, which is probably a continuation, returns to the value of 9° at greater radii. Arm 6 deviates considerably from the average spiral geometry.

Roberts, Roberts & Shu (1975) argue that, for the density-wave model, the speed Ω_p at which the spiral pattern rotates, and hence the corotation radius (at which $\Omega_p = \Omega(R)$, where $\Omega(R)$ is the angular velocity of rotation for gas in the disc), influence the radial extent of the prominent spiral structure and of the 'easily visible' disc. Their choice for the corotation radius is therefore coincident with the extent of the easily visible disc, giving a value of 12.5 kpc for IC342 with a corresponding value of $\Omega_p = 15$ km s^{-1} kpc^{-1} derived from the rotation curve. Although H I spiral structure extends far beyond the optical disc, it is unlikely in the density-wave model that spiral arms will persist through the corotation region unaffected. There is evidence from the present observations for a break between the inner arms, which coincide with the easily visible optical spiral structure, and the outer H I arms (Fig. 3). Arms 2, 3 and 8 in particular begin rather abruptly and cannot easily be related to the inner features. The break lies between 12 and 16 arcmin from the nucleus and, if this is interpreted as the corotation region, a pattern speed $9 < \Omega_p < 12$ km s^{-1} kpc^{-1} is implied. This is considerably less than the value of 20 km s^{-1} kpc^{-1} adopted for M81 (Rots & Shane 1975) but similar to that of 11 km s^{-1} kpc^{-1} derived for M31 by Guibert (1974).

4 Relation between H I and other Population I material

4.1 H I AND OPTICAL EMISSION

Optical information about IC342 is very limited because of the large extinction, 2.2 mag in the blue (Ables 1971). The most detailed study is Ables' photometric survey, where the galaxy was found to have spiral arms of unusually low surface-brightness in contrast with the bright nucleus. A 48-inch Schmidt photograph of IC342 taken in blue light is shown in Plate 3 with peak contours from the high-resolution H I map superimposed. Optical spiral structure extends to $R \simeq 10$ arcmin; it is multi-armed, branching from a basic two-armed pattern which emerges from the nuclear region.

There is good correlation between peaks of H I emission and optical features. The inner H I spiral segments indicated on Fig. 3 correspond with the outer optical arms, but the best correlation is found for the feature labelled 9 on Fig. 3; it follows a distinctive optical arm for ~ 26 arcmin (35 kpc). There is no evidence for any systematic displacement of the H I either to the inside or the outside of the optical arms.

Although the best-defined H I spiral arms lie beyond the clear optical structure, an area of diffuse optical emission is visible on Palomar Observatory Sky Survey plates in a region of high H I surface brightness at RA $03^h\,41^m$, $\delta\,67°\,42'$ along arm 2. The emission lies beyond the outer isophote measured by Ables (1971), but the coincidence with H I suggests that it belongs to IC342 and that stellar spiral structure is present at large radii.

The correlation between H I and dust has been well established for other spiral galaxies. Several dust lanes are visible towards the centre of IC342 ($R < 5$ arcmin, e.g. Fig. 1 of Morris & Lo 1978), but most of the dust 'structure' lies within the H I-deficient region. The clearest dust lanes outside this region are associated with an optical arm 4.5 arcmin north-west of the nucleus and this indeed coincides with an H I ridge (11) having $\int T_b\, dv$ values reaching 500–600 K km s^{-1}. Dust in the outer arms would be difficult to observe against the corresponding faint optical emission.

4.2 COMPARISON WITH RADIO CONTINUUM DATA

Fig. 4 shows the 1.9 x 2.0 arcmin resolution map of continuum emission in a 10-MHz band centred on 1419.0 MHz derived from the present observations. H I emission has been subtracted and an unresolved source at the nucleus removed. Table 2 gives the details of unresolved sources detected in the IC342 field.

The clearest spiral feature on Fig. 4 again corresponds to the H I arm labelled 9 on Fig. 3. The continuum arm correlates well with the H I feature and may be traced from the south-west major axis to the north-east major axis, reaching a distance of ~ 12 arcmin from the nucleus.

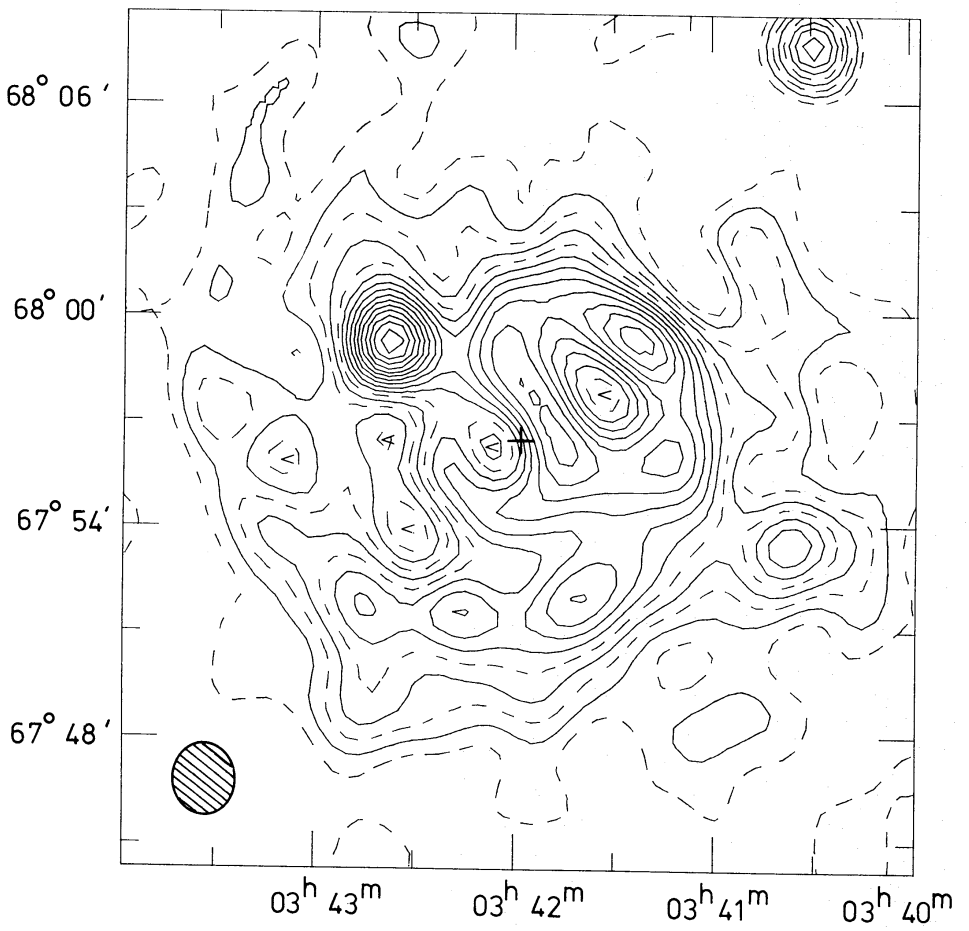

Figure 4. Broadband continuum map of the IC342 field, centred on 1419.0 MHz, at 1.9 X 2.0 arcmin resolution. The contour interval is 4 mJy per beam area at the map centre, starting from 4 mJy per beam area. The lower contours are shown alternately dashed and solid. The rms noise level is 1.5 mJy per beam area. H I emission has been subtracted from the map and an unresolved source at the nucleus removed. The map is not corrected for the primary beam response.

Table 2. Positions and flux densities of unresolved sources at 1419.0 MHz in the IC342 field.

Source number	RA (1950.0) h m s	DEC (1950.0) ° ′ ″	Flux density (mJy)	
1	03 35 04.0	67 59 16	51.6	
2	03 36 14.1	67 17 40	130.4	
3	03 36 41.7	67 51 38	322.9	4C 67.08
4	03 36 54.6	67 41 15	157.4	4C 67.08
5	03 37 44.7	68 35 14	175.1	
6	03 38 07.7	67 08 46	237.0	
7	03 39 48.3	68 18 19	68.0	
8	03 40 29.5	68 07 33	34.5	
9	03 41 58.8	67 56 30	178.2	Nucleus
10	03 42 10.3	68 35 46	86.5	
11	03 42 36.9	67 59 26	53.7	
12	03 43 06.1	67 12 04	205.9	
13	03 43 18.2	68 22 36	66.1	
14	03 47 29.9	67 49 33	436.0	4C 67.09
15	03 47 52.8	68 00 54	70.4	

Fig. 4 is in good overall agreement with the 1415-MHz map at a resolution of 1 arcmin by van der Kruit (1973). Van der Kruit found the radio spiral arms to be displaced to the inner edge of the bright optical emission and to be coincident with dust lanes where visible. The arms have a non-thermal spectral index ($\alpha > 1.0$, Baker *et al.* 1977). This result is consistent with the internal structure of a spiral arm (within the corotation radius) predicted by the non-linear density-wave theory (e.g. Roberts & Yuan 1970), where a shock, an H I peak, a dust lane and a non-thermal radio continuum peak are all expected to lie in a narrow compression region on the inside edge of the optical arms. At the resolution of the present survey there is no systematic displacement between the H I and continuum ridges of emission along the eastern part of arm 9. In the south, the H I and optical emission are displaced to the outside of the continuum ridge, apparently in conflict with the density-wave prediction, but the comparison is confused in this area by the central H I depletion; hydrogen may be present along the continuum ridge but in molecular form (Section 4.3). The morphology of arm 9 is therefore consistent with the predictions of density-wave theory within the limitations imposed by the angular resolution of the present survey.

As a consequence of the high optical obscuration, there are no detailed surveys of H II regions in IC342. Fig. 5, however, shows the relation between the H I distribution and the positions of 10 discrete radio sources identified by Baker *et al.* (1977) as probable concentrations of H II regions. They are all coincident with optical and H I spiral features, although on a smaller scale they tend to lie around the edge of H I peaks. Similar small-scale anti-correlations found for other galaxies from optically defined samples of H II regions have been explained as due to obscuration by dust in regions of strong H I emission (e.g. Madore, van den Bergh & Rogstad 1974). This explanation is not applicable to radio emission, but a more detailed survey of H II regions in IC342 is required before the significance of the effect may be determined.

4.3 CO EMISSION

CO emission from IC342 has been detected and its distribution partially determined by Morris & Lo (1978). The circles marked on Fig. 5 indicate the positions at which

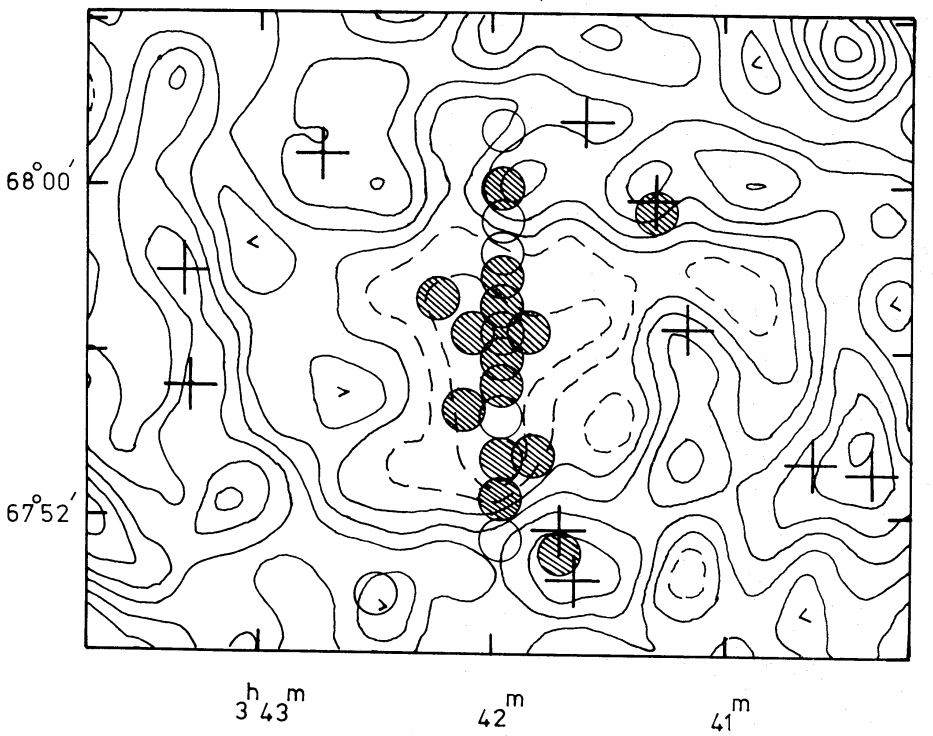

Figure 5. Contours of integrated H I emission from IC342 at 1.9 × 2.0 arcmin resolution, with the positions of probable concentrations of H II regions (Baker *et al.* 1977) marked by crosses. Circles represent the positions of observations of CO emission by Morris & Lo (1978); shaded circles indicate detections. The contour interval is 100 K km s^{-1} with dashed contours at 100 and 200 K km s^{-1}.

observations were made, and represent the 65-arcsec FWHP resolution of the survey. CO emission was detected in the outer optical arms but found to peak in the nuclear region. There are seven observations outside the central H I depletion area ($\int T_b dv > 200$ K km s^{-1}). With the exception of the extreme south-east point, CO detections are coincident with H I peaks, whereas points where no detection was made coincide with H I minima. Detections occur for H I surface densities of 9.0–10.8 × 10^{20} atom cm^{-2} ($\equiv$ 8.1–9.7$M_\odot$ pc^{-2} in the plane of IC342 at 4.5 Mpc). Morris & Lo estimate a similar value for the total surface density of molecular material in these regions. The beamsize of the H I survey is twice that of the CO observations, so that the values are not directly comparable and the H I surface densities are lower limits. The present survey yields an upper limit of 2.4$M_\odot$ pc^{-2} for the average surface density of H I in the nuclear region where Morris & Lo estimate a corresponding value of 50$M_\odot$ pc^{-2} for molecular material. These observations are therefore consistent with the conclusions of the latter authors that there is no central depletion in the *total* surface density of hydrogen gas (H I + H_2) and that it probably reaches a maximum across the nuclear region.

5 Velocity dispersion

Dispersions (FWHP) of the line profiles observed at 1.9 × 2.0 arcmin resolution lie mainly in the range 25–35 km s^{-1}, except in regions with high gradients in radial velocity or H I intensity, where the gradients affect profile widths. Values of dispersion measured along the major and minor axes are shown in Fig. 6 using both high- and low-resolution data. Along the major axis, beam-smearing effects are small, apart from the region of high velocity-gradient near the nucleus. For $R > 5$ arcmin, the dispersion values are approximately

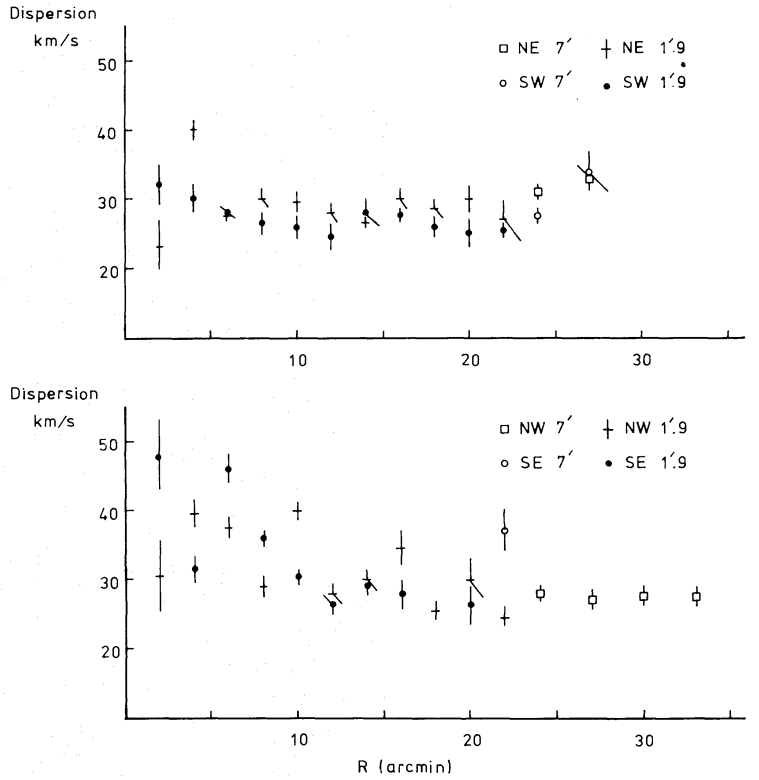

Figure 6. Observed FWHP velocity dispersion of the H I gas along the major (a) and minor (b) axes of IC342, uncorrected for the instrumental broadening.

constant to the edge of detected H I emission, and a value of 28 ± 3 km s^{-1}, independent of radius, is derived. Along the minor axis, where beam-smearing becomes more significant, observed dispersions decrease from ~ 40 km s^{-1} at $R = 5$ arcmin to ~ 30 km s^{-1} at $R = 20$ arcmin and ~ 27 km s^{-1} at greater radii in the north-west. Allowing for the effects of beam-smearing, these values are consistent with the major-axis measurements and there is no evidence for a variation of dispersion with radius.

The value of 28 km s^{-1} corresponds to 23 km s^{-1} after correction for instrumental broadening, giving a rms value of 9.8 km s^{-1} for a Gaussian distribution. This is in excellent agreement with values obtained for other spiral galaxies e.g. our own Galaxy (van Woerden 1967), M31 (Emerson 1976) and M33 (Newton 1980a).

The thickness (z) of the H I layer in the plane of IC342 has been estimated (Newton 1978) by assuming the above value for velocity dispersion and following the method described by Emerson (1976). The variation of z is approximately linear from $z = 400$ pc at radius $R = 5$ kpc to $z = 1800$ pc at $R = 40$ kpc. This is similar to the variation calculated for M31 by Emerson (1976) for $R < 28$ kpc.

For $12 < R < 20$ arcmin, the mean surface density of 6.0×10^{20} H atom cm^{-2} derived from Fig. 2 corresponds to a mean space density of 0.3 H atom cm^{-3}, assuming a mean disc thickness of 700 pc.

6 The radial-velocity field

The low-resolution (7.0×7.6 arcmin) data shown in Paper I give the best indication of the *average* disc parameters and the values summarized in Section 1 of the present paper are

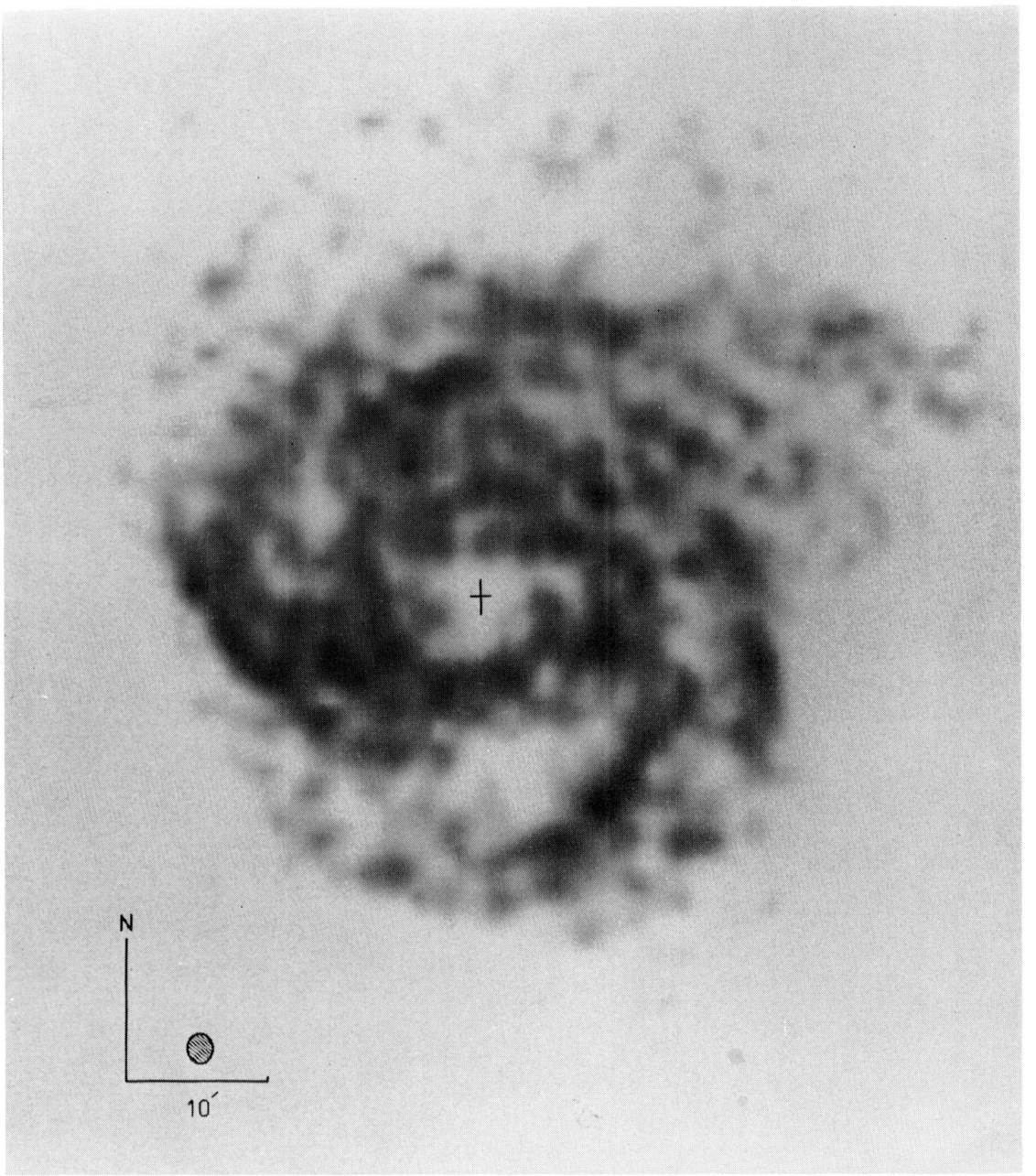

Plate 1. A photographic representation of the integrated H I emission from IC342 at 1.9×2.0 arcmin resolution. The nucleus is marked by a cross.

[*facing page* 624]

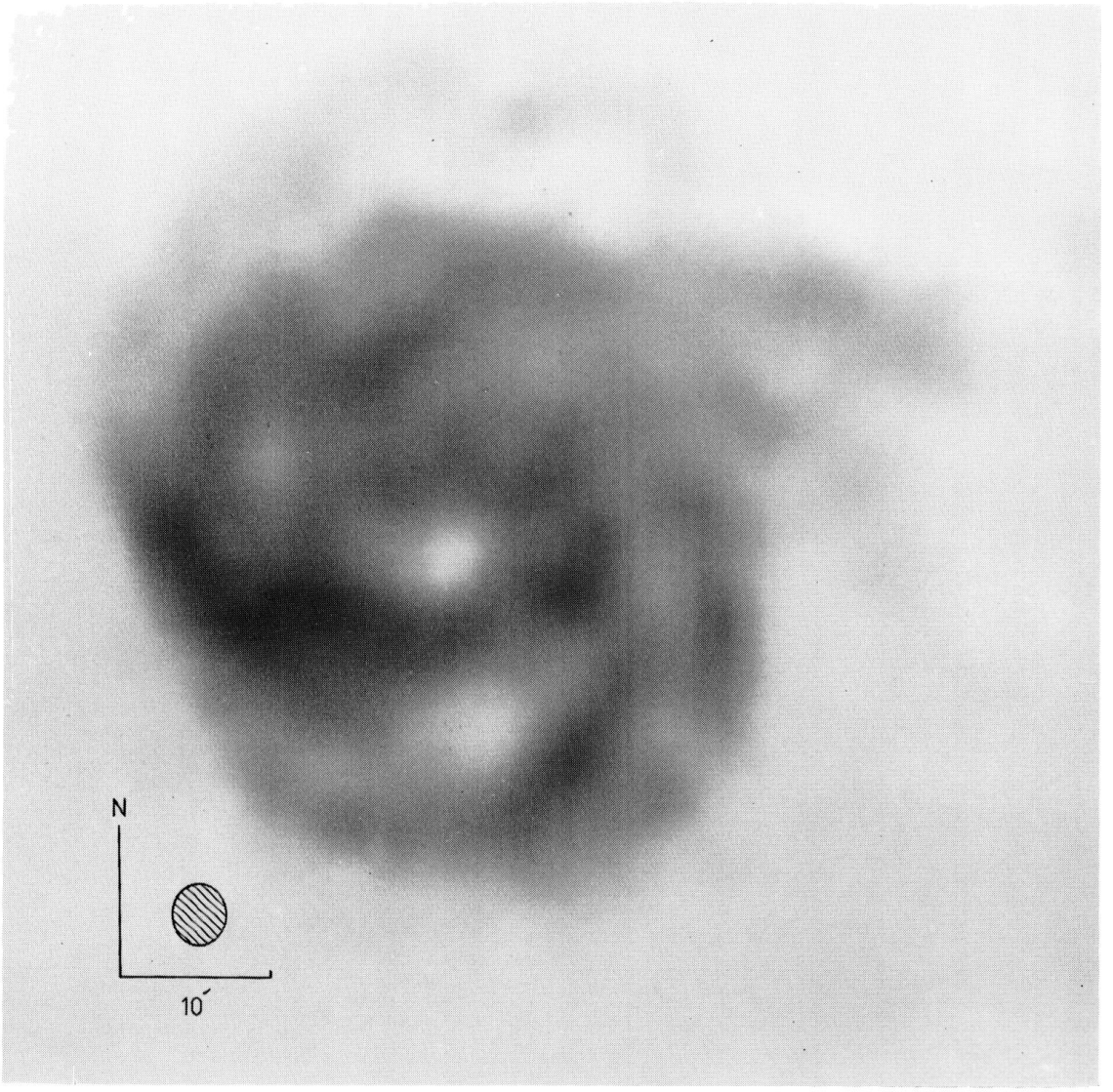

Plate 2. Integrated H I emission from IC342 with an angular resolution of 3.6 × 3.9 arcmin.

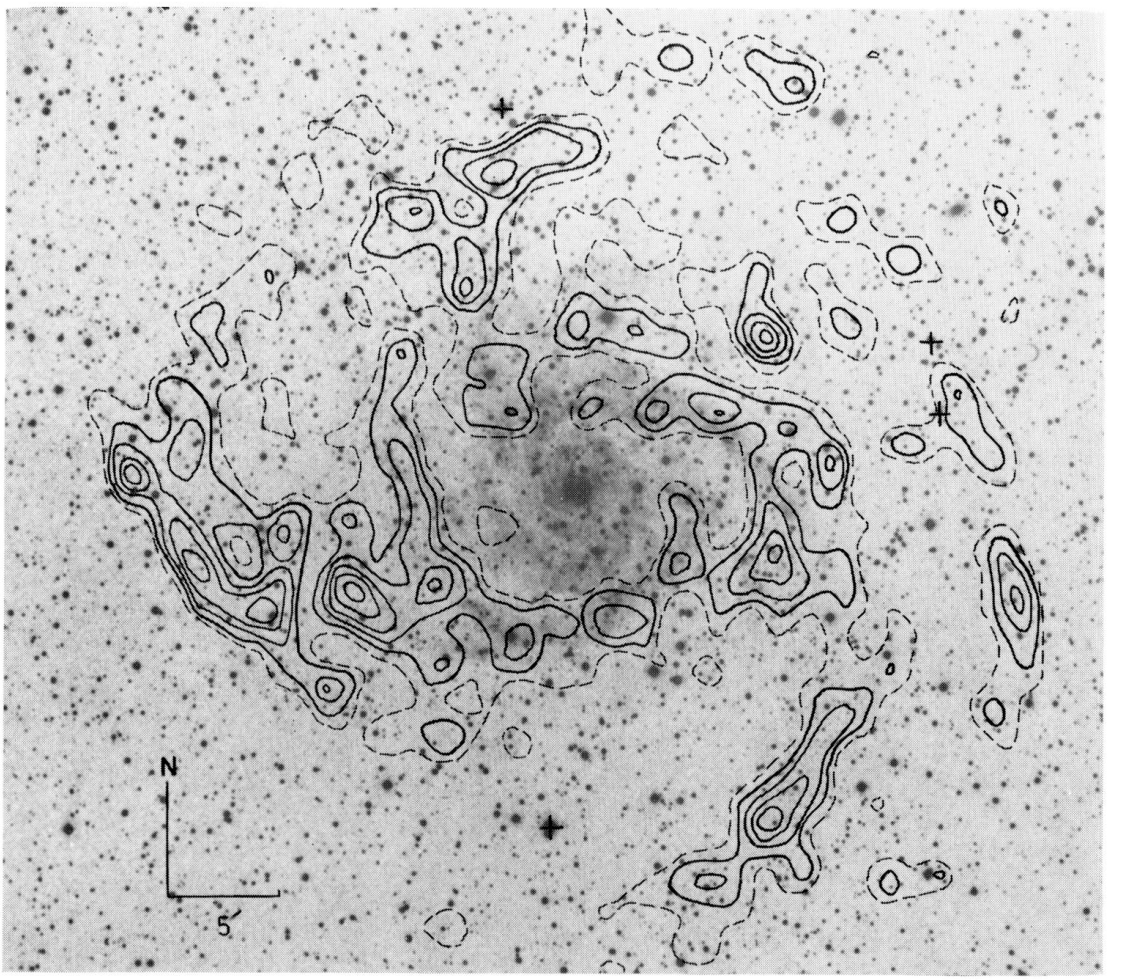

Plate 3. Peak contours of integrated H I emission superimposed on an optical photograph taken in blue light. The contour interval is 100 K km s^{-1} and the dashed contour is at 400 K km s^{-1}. Photograph copyright by the National Geographic Society—Palomar Observatory Sky Survey. Reproduced by permission from the Hale Observatories.

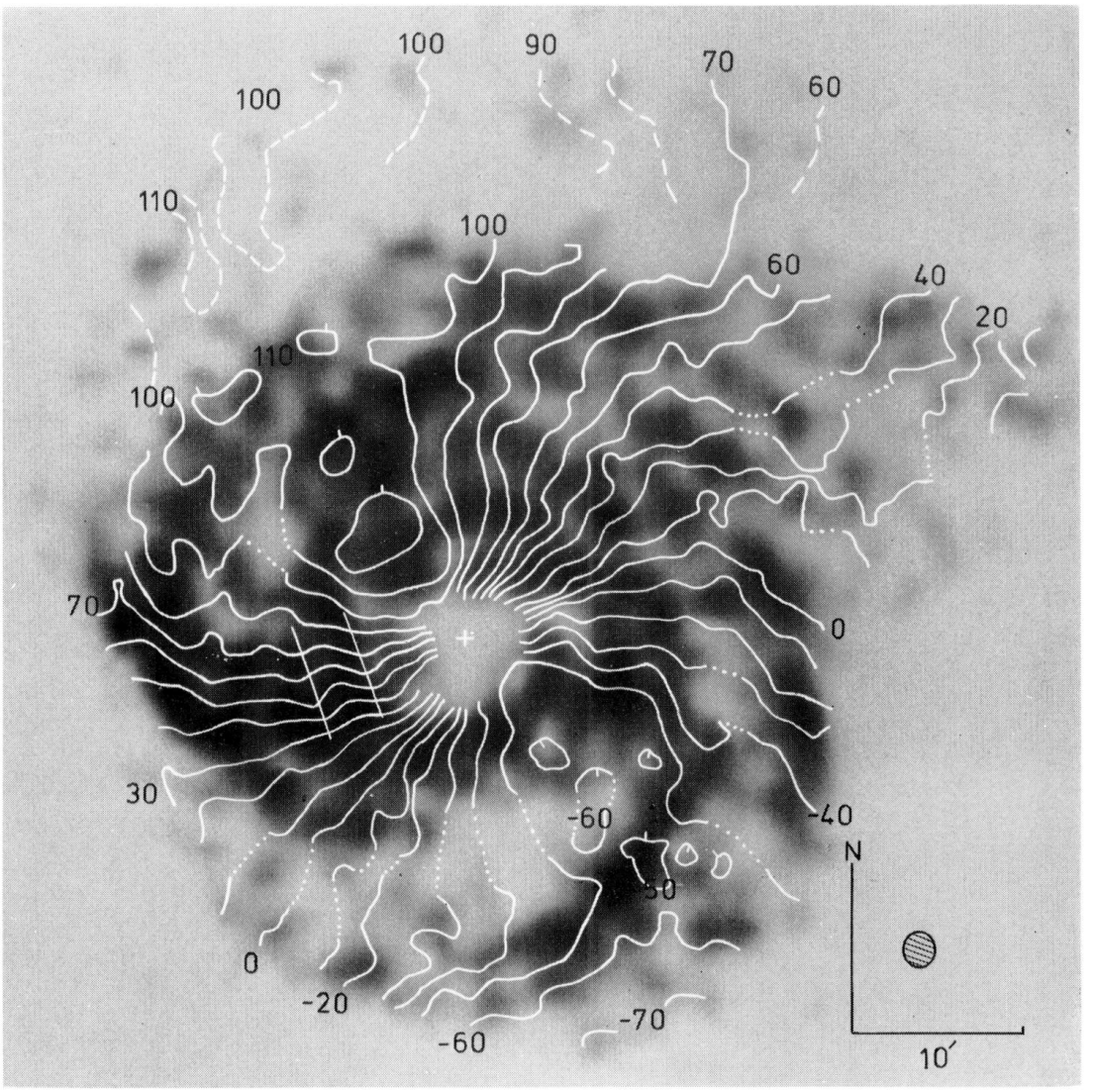

Plate 4. IC342 : The radial velocity map at 1.9×2.0 arcmin resolution superimposed on an optical representation of the integrated H I emission. The contour interval is 10 km s^{-1}; uncertain velocities are shown dotted and dashed contours are taken from the data at 3.6×3.9 arcmin resolution.

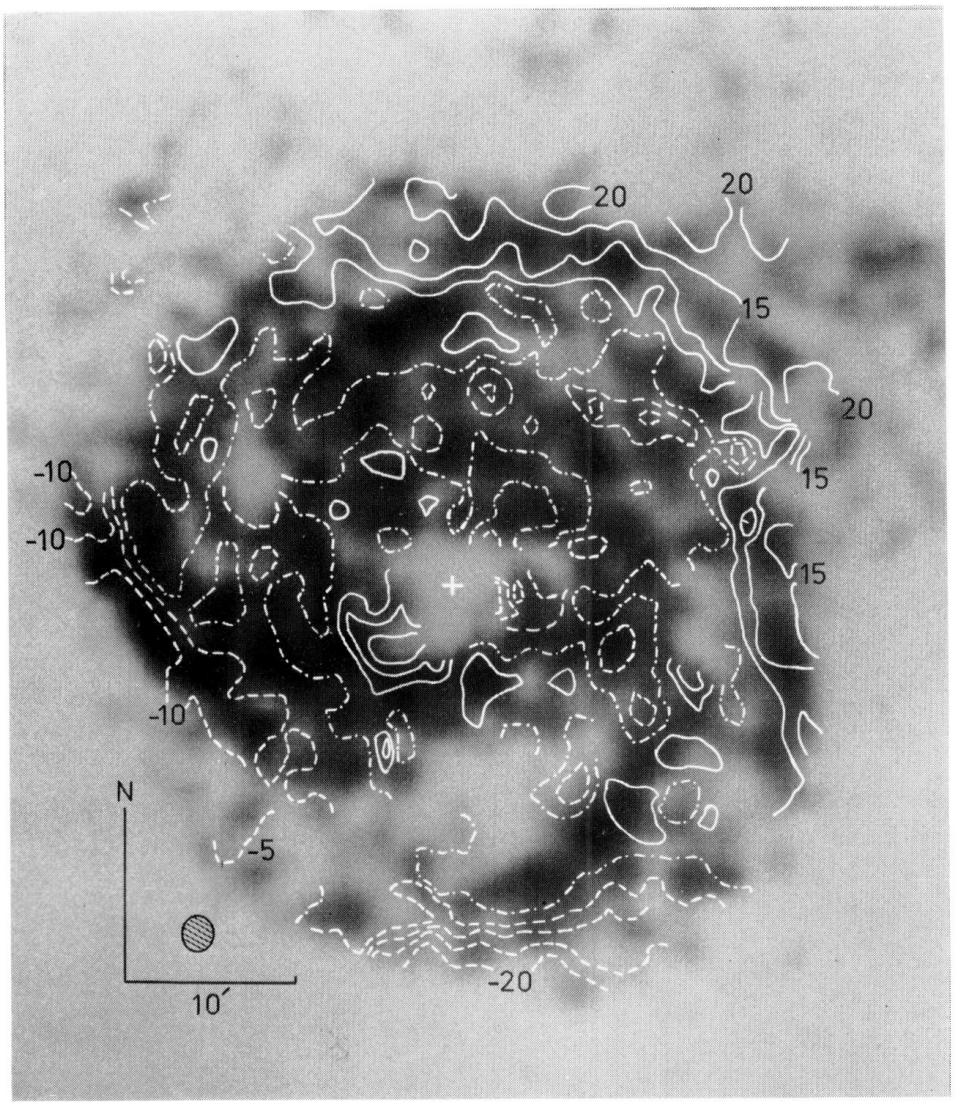

Plate 5. IC342 : residual velocity field. This shows the result of subtracting the velocities calculated from a flat disc model from the observed radial-velocity field at 1.9×2.0 arcmin resolution for $R < 30$ arcmin. The contour interval is 5 km s^{-1}, negative contours – – –; zero contour –·–·–; positive contours ———.

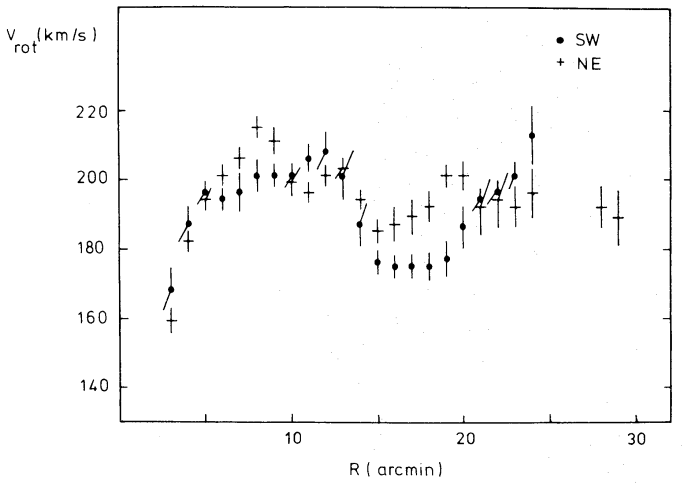

Figure 7. Major-axis rotation velocities, derived from the radial velocity field at 1.9 × 2.0 arcmin resolution and assuming disc parameters given in the text.

assumed. The radial-velocity field at 1.9 x 2.0 arcmin resolution is shown in Plate 4. The overall pattern is remarkably smooth and continuous, revealing normal differential rotation in the central region with perturbations in the outer parts. Dashed contours to the north are taken from the data at 3.6 x 3.9 arcmin resolution (Plate 2); these velocities are in good agreement with the high-resolution values where measured. The major-axis rotation curve, constructed from Plate 4, is shown in Fig. 7. Deviations from normal circular rotation are indicated by the residual velocity field, which displays the difference between observed and model velocities (Plate 5). The model consists of a flat disc with the parameters given in Section 1, in circular rotation and having the rotation curve in Fig. 7 for $R < 16$ arcmin, with a constant $V_{\rm rot} = 191$ km s^{-1} at greater radii. There are large residuals (> 15 km s^{-1}) both in the central region and in the outer parts of the galaxy.

6.1 LARGE-SCALE PERTURBATIONS

The warp model presented in Paper I remains a good fit to the average velocity field at high resolution and accounts for perturbations in the outer parts of the disc for $16' < R < 25'$. The low resolution data showed that perturbations in the north-west apparently decrease at larger radii and are not consistent with a simple extrapolation of the model. The high-resolution maps show the anomalies to be confined mainly to arms 4 and 6. Residual velocities decrease from ~ 20 km s^{-1} at the inner end of arm 6 to zero at the outer end, while residuals along arm 4 *increase* from zero at $R = 30$ arcmin in the north-east to ~ 15 km s^{-1} in the north-west at $R = 36$ arcmin. Similarly, residuals decrease to zero towards the end of arm 2 in the south.

Spiral arms extend over the warped part of the disc and, if the rotation curve is approximately flat at large radii, the 'corrugation' of the disc is complex. It is difficult, in the light of present theories of spiral structure at least, to explain the persistence of spiral arms where there are large motions perpendicular to the plane. The suggestion made in Paper I that the warp is the result of a tidal interaction with a companion for IC342 recently discovered by Rots (1979) is therefore attractive. In this picture, the arms could have been warped away from the plane recently, or they may indeed result from the interaction itself in a manner similar to the origin of the outer arms in M51 proposed by Toomre & Toomre (1972).

6.2 ANOMALOUS VELOCITIES IN THE CENTRAL REGIONS

Assuming that large-scale perturbations across the outer region in Plate 4 result from warping of the plane, the velocity field may be examined for additional small-scale structure. Fig. 8 shows observed line-of-sight velocities along the major (a) and minor (b) axes, where tangential and radial components of velocity in the plane of the galaxy are separated, together with the integrated H I density profile from Fig. 1.

Fig. 8(b) shows peculiar velocities along the minor axis between radii of 3 and 7 arcmin, especially in the south-east where perturbations reach 16 km s^{-1}, and Plate 5 also shows large residuals (> 15 km s^{-1}), in the western quadrant at these small radii. A contribution to these anomalies could come from the broad velocity profiles in these areas, since the profiles are distorted both by the high gradient in radial velocity around the nucleus and by the gradient in H I emission. The corresponding effects on measured velocities are discussed by Warner, Wright & Baldwin (1973), but it is unlikely that these effects can explain all of the observed perturbations. If the perturbations are representative of the true behaviour of the H I gas, then the kinematic south-east minor axis is not perpendicular to the major axis.

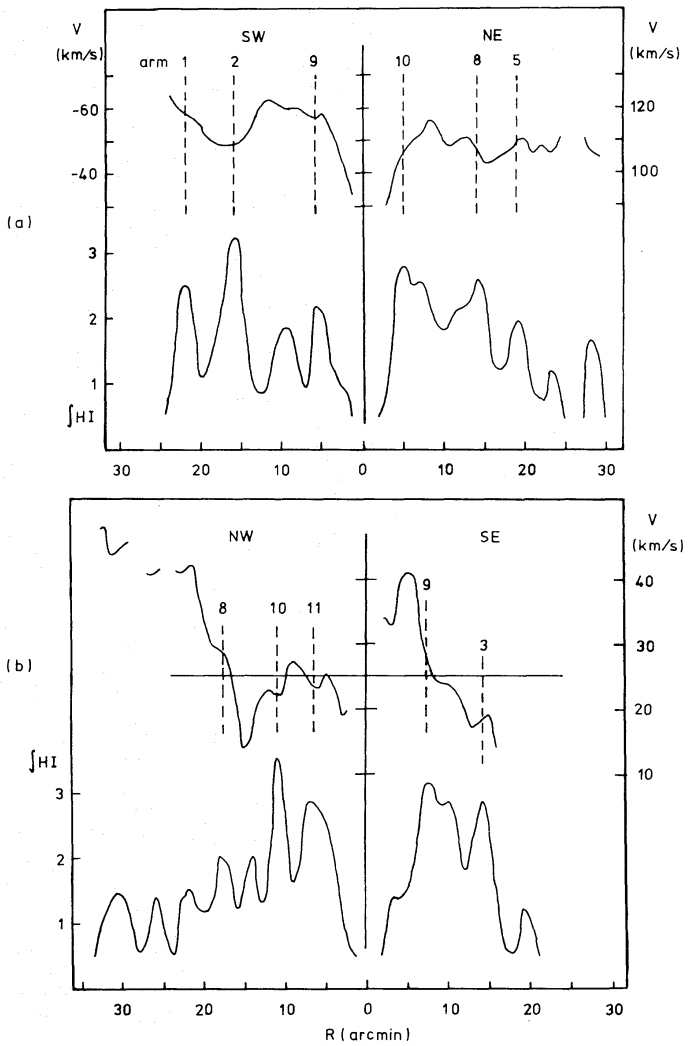

Figure 8. Observed velocities along the major (a) and minor (b) axes of IC342 from the data at 1.9 × 2.0 arcmin resolution shown in Plate 4, together with the integrated H I column density after correction for the primary beam response, shown in arbitrary units.

Such non-orthogonality has been observed in the inner regions of several galaxies and can result from oval structures in an otherwise planar disc, e.g. bars (Bosma 1978). However, this would be expected to give rise to symmetrical deviations in radial velocity over the disc, which is not the case in IC342. More likely explanations are either (i) local warping of the inner disc or (ii) that the disc has the same orientation as at greater radii, but the H I is moving with peculiar velocities. In the former case, perturbations near the south-east minor axis correspond to a change in orbit position angle of $\sim 14^\circ$ at $R \simeq 5$ arcmin (similar to the change in p.a. of the minor axis in the outer parts of the disc for the warp model described in Paper I). Any such distortion would be confined to the vicinity of the minor axis, since there is no evidence for a variation of *major* axis p.a. at these small radii. In the latter case, on the assumption that the observed spiral arms are trailing features and the north-west edge of IC342 is nearest to us, the sense of the minor-axis velocity perturbations corresponds to a radial expansion component, in the plane of the disc, reaching 34 km s^{-1} in the south-east.

Such interpretations are not unreasonable in view of evidence for radial expansion in the central regions of our own Galaxy (reviewed by Oort 1977) and observations indeed indicate the layer of expanding H I to be inclined to the galactic equator (van der Kruit 1970; Cohen & Davies 1976), giving a combination of (i) and (ii) above. H I with anomalous velocities has also been detected near the nucleus of M31 (Whitehurst & Roberts 1972; Emerson 1976) and there is good evidence for large-scale non-circular motions of gas in the nuclear regions of other spiral galaxies e.g. Burbidge (1970); Sanders & Bania (1976).

6.3 VELOCITY PERTURBATIONS AND SPIRAL STRUCTURE

Although the face-on inclination of IC342 enables the spiral arms to be easily separated, this orientation has the disadvantage that the line-of-sight component of velocity perturbations in the plane of the disc is considerably reduced. The velocity field (Plate 4) contains considerable fine structure, much of which may be ascribed to the rms noise of 1–4 km s^{-1}. After allowing for the large-scale deviations, there are no small-scale perturbations > 5 km s^{-1} associated with the spiral arms.

Comparisons have often been made between observed velocity fields of spiral galaxies and the predictions of density-wave theory (e.g. Lin, Yuan & Shu 1969), usually by assuming a two-armed spiral pattern. It is unlikely that the simple theory is representative of the gas dynamics in IC342 since (i) the spiral pattern is multi-armed over the entire H I disc and (ii) warping of the outer arms would result in motions perpendicular to the plane of the disc. Nevertheless, if the spiral features are indeed 'quasi-stationary' wave phenomena, we might expect to find associated velocity perturbations.

An estimate of the magnitude of perturbations in the radial component of velocity inside an arm may be derived by considering a *narrow* arm which forms part of a stationary density-wave pattern in a frame rotating with angular velocity Ω_p. The resulting expression for the perturbation (Newton 1980a) is

$$V_r \simeq \left(1 - \frac{\sigma_{\text{disc}}}{\sigma_{\text{arm}}}\right) R\,[\Omega_p - \Omega(R)] \tan t,$$

of which the line-of-sight component is

$$(V_r)_{\text{obs}} = V_r \sin i \sin \theta,$$

where σ is the gas density, R the distance to the centre, $\Omega(R)$ the gas rotation velocity, t the pitch angle of the spiral arm, i the inclination of the disc and θ, angle in the plane of the disc measured relative to the major axis.

The perturbation corresponds to an *apparent* motion towards the nucleus within an arm and away from the nucleus in interarm regions. The directions of these motions are reversed beyond the corotation radius (R_c). Values of $V_r \sin i$ (the observed perturbation along the minor axis) calculated for different radii and pattern speeds are given in Table 3, assuming $t = 9°$, $i = 25°$ and $(1 - \sigma_{disc}/\sigma_{arm}) = 1$.

With corotation at 6 kpc ($\Omega_p = 30$ km s^{-1} kpc^{-1}), Table 3 indicates perturbations > 30 km s^{-1} in the outer arms. Since no large radial perturbations are observed on the scale of the arms, it is unlikely that corotation is at so small a radius. There are many perturbations in the disc with magnitudes of a few km s^{-1}, but their sense often changes over short distances along the arms and, with the possible exception of arm 9, there is no evidence for *systematic* deviations. This is consistent with Table 3 for corotation at a larger radius. With $R_c = 20$ kpc ($\Omega_p = 9$ km s^{-1} kpc^{-1}), estimated perturbations are < 4 km s^{-1} over most of the disc, and even less for smaller contrast ratios – perturbations are then comparable with the noise level. Although a still larger corotation radius cannot be ruled out, these calculations are also consistent with the earlier estimate, based on the H I distribution, of $16 \lesssim R_c \lesssim 21$ kpc (Section 3), with a corresponding $\Omega_p \simeq 10$ km s^{-1} kpc^{-1}.

More direct evidence for the presence of a density-wave in IC342 is derived from the marginal detection of systematic velocity perturbations along the well defined inner arm (9). The perturbations lie immediately to the north of the minor axis at $R \simeq 7.5$ arcmin (10 kpc), along the brightest part of the arm; the region is indicated by parallel lines on Plate 4. The morphology of the arm has already been shown to conform to predictions of the density-wave theory (van der Kruit 1973; Section 4.2). 'Wiggles' in the isovelocity contours extend along the arm for 6.5 arcmin and have peak-to-peak magnitudes of ~ 5 km s^{-1}; the rms noise for velocities near the ridge is ~ 1.5 km s^{-1}. The sign of these perturbations agrees with the above calculations for radii within corotation, and strengthens the argument in favour of a small pattern speed.

Perturbations of gas velocity in the disc would be expected near a spiral arm, whether or not it is a quasi-stationary wave, due to the additional gravitational acceleration produced by the excess mass in the arm. This effect is nearly tangential because of the small pitch angle of the arms, and corresponds to an increase of V_{rot} outside an arm with a decrease along the inside edge. Fig. 8(a) shows some velocity structure on the scale of the arms along

Table 3. Predicted amplitude of the radial component (in the plane of the galaxy) of velocity perturbations along a narrow spiral arm in IC342, derived by assuming the parameters given in Section 1. (Negative values correspond to an apparent radial contraction of gas in the arm relative to the interarm gas.)

Radius (kpc)	$V_r \sin i$ (km s^{-1})		
	Corotation radius (kpc) = 39	20	6
	Ω_p (km s^{-1} kpc^{-1}) = 5	9	30
5	−10.4	−8.1	−2.0
10	−10.3	−7.6	6.4
15	−8.5	−4.5	16.6
20	−5.4	−0.5	28.0
25	−4.4	2.3	37.4
30	−3.1	5.0	47.1
35	−1.3	8.0	57.2
40	0.4	11.1	67.3

the major axis, where the rotational component is isolated, but again no systematic perturbations are visible. A calculation of the magnitude of expected perturbations, by considering the self-gravity of the H I gas alone, predicts an observed peak-to-peak perturbation of ~ 3 km s^{-1} across the brighter arms (Newton 1978). The magnitude may be increased if a significant mass is present in other forms, but this factor is unlikely to be important at large radii and again the expected deviations are comparable with the noise level of the present observations.

This survey has therefore provided some evidence for the presence of density-waves in the inner parts of IC342, supporting that derived from the distribution of the continuum (van der Kruit 1973). The most likely pattern speed is ~ 10 km s^{-1} kpc^{-1} with corotation at $R \approx 20$ kpc. If the outer arms are quasi-stationary waves with a similar pattern speed, then velocity perturbations, both radial and tangential, with magnitudes 2–4 km s^{-1} are predicted. Such motions would not be detected by the present observations but should be observable using existing aperture synthesis techniques.

7 Conclusions

(1) Neutral hydrogen emission from IC342 has been resolved into high-contrast spiral arms, which extend to the limit of detected H I at $R \simeq 50$ kpc. The spiral pattern is multi-armed and the arms are often unresolved in width, implying true widths less than 2.5 kpc.

(2) The H I correlates well with other Population I material in the inner parts of the galaxy, but the clearest H I spiral arms lie beyond the optical emission.

(3) Anomalous velocities of the H I observed towards the nucleus indicate the presence of non-circular motions which may be associated with the large-scale expulsion of gas from the central region.

(4) Large-scale velocity perturbations in the outer regions are in good agreement with the galactic warp model described in Paper I. The outer spiral arms, which have typical lengths of 40 kpc, therefore appear to be warped away from the plane of the central disc.

(5) Direct evidence for the presence of a density-wave in IC342 is derived from both the structure of, and a marginal detection of velocity perturbations along, the inner arm labelled 9 on Fig. 3. The velocity perturbations are consistent with the pattern speed $\Omega_p \simeq 10$ km s^{-1} kpc^{-1} derived from the overall H I distribution.

(6) There are no systematic velocity perturbations with magnitude > 5 km s^{-1} associated with the spiral arms elsewhere in the disc. If the arms are 'quasi-stationary' waves, the absence of large radial streaming motions also implies a small pattern speed ($\Omega_p \lesssim 10$ km s^{-1} kpc^{-1}) in which case perturbations of order 2–4 km s^{-1}, comparable to the rms noise level, are predicted over most of the disc.

Acknowledgments

I am grateful to many members of the Radio Astronomy Group for assistance with the observations and data analysis. I particularly thank Mr P. J. Warner for invaluable advice and Drs J. E. Baldwin and J. R. Shakeshaft for helpful discussions and comments on the manuscript. Financial support from the SRC and the Royal Commission for the Exhibition of 1851 is gratefully acknowledged.

References

Ables, H. D., 1971. *Publs U.S. Naval Obs. Sec. Ser.* Vol. **XX**, Part IV, Washington, D.C.
Baker, J. R., Haslam, C. G. T., Jones, B. B. & Wielebinski, R., 1977. *Astr. Astrophys.*, **59**, 261.

Bosma, A., 1978. *PhD thesis,* University of Groningen.
Burbidge, G. R., 1970. *A. Rev. Astr. Astrophys.*, **8**, 369.
Cohen, R. J. & Davies, R. D., 1976. *Mon. Not. R. astr. Soc.*, **175**, 1.
Emerson, D. T., 1976. *Mon. Not. R. astr. Soc.*, **176**, 321.
Guibert, J., 1974. *Astr. Astrophys.*, **30**, 353.
Lin, C. C., Yuan, C. & Shu, F. H., 1969. *Astrophys. J.*, **155**, 721.
Madore, B. F., van den Bergh, S. & Rogstad, D. H., 1974. *Astrophys. J.*, **191**, 317.
Morris, M. & Lo, K. Y., 1978. *Astrophys. J.*, **223**, 803.
Newton, K., 1978. *PhD thesis,* University of Cambridge.
Newton, K., 1980a. *Mon. Not. R. astr. Soc.*, **190**, 689.
Newton, K., 1980b. *Mon. Not. R. astr. Soc.*, **191**, 169.
Oort, J. H., 1977. *A. Rev. Astr. Astrophys.*, **15**, 295.
Roberts, M. S., 1967. *Proc. IAU Symp. No. 31,* p. 189, Academic Press, New York.
Roberts, W. W., Roberts, M. S. & Shu, F. H., 1975. *Astrophys. J.*, **196**, 381.
Roberts, W. W. & Yuan, C., 1970. *Astrophys. J.*, **161**, 887.
Rogstad, D. H., Wright, M. C. H. & Lockhart, I. A., 1976. *Astrophys. J.*, **204**, 703.
Rots, A. H., 1979. *Astr. Astrophys.*, in press.
Rots, A. H. & Shane, W. W., 1975. *Astr. Astrophys.*, **45**, 25.
Sanders, R. H. & Bania, T. M., 1976. *Astrophys. J.*, **204**, 341.
Toomre, A. & Toomre, J., 1972. *Astrophys. J.*, **178**, 623.
Unwin, S. C., 1980. *Mon. Not. R. astr. Soc.*, **190**, 551.
van der Kruit, P. C., 1970. *Astr. Astrophys.*, **4**, 462.
van der Kruit, P. C., 1973. *Astr. Astrophys.*, **29**, 249.
van Woerden, H., 1967. *IAU Symp. No. 31,* p. 3, ed. van Woerden, H., Academic Press, New York.
Warner, P. J., Wright, M. C. H. & Baldwin, J. E., 1973. *Mon. Not. R. astr. Soc.*, **163**, 163.
Whitehurst, R. N. & Roberts, M. S., 1972. *Astrophys. J.*, **175**, 347.

Appendix 1

The microfiche with this paper (*Microfiche* MN 191/1) shows the continuum-free spectrometer output maps of H I emission, at 1.9 x 2.0 arcmin resolution and over the heliocentric radial-velocity range 156.2 to -107.6 km s^{-1}. Details of the maps are given in Table 1. No correction for the primary beam response of the telescope has been applied, so that the rms instrumental noise level is uniform over the maps. The contour interval is 3 K at the map centres, with the first contour (3 K) shown dashed. Negative and zero contours have been omitted. The map centres are indicated by large crosses, and small crosses indicate the positions of bright foreground stars, which are given in Table 4. Map coordinates (1950.0) are given in hours, minutes and seconds (RA) and degrees, minutes and seconds of arc (δ).

Table 4. Star positions indicated in Appendix 1.

	RA (1950)	DEC (1950)
	h m s	° ′ ″
1	03 34 43.84	67 19 30.27
2	03 34 58.83	68 08 37.61
3	03 35 22.42	68 06 26.15
4	03 39 55.17	68 39 48.23
5	03 42 12.38	67 41 36.24
6	03 43 04.22	68 30 56.67
7	03 46 45.67	68 21 26.74
8	03 47 45.66	67 24 26.33
9	03 47 48.21	67 44 40.59

Monthly Notices
of the
ROYAL
ASTRONOMICAL SOCIETY

VOL. 191, NO. 2, 1980

K. Newton

Neutral hydrogen in IC 342 - II
The detailed structure

Published for
the Royal Astronomical Society
by
Blackwell Scientific Publications Ltd
Osney Mead
Oxford
OX2 0EL

The microfiches are 105 × 148mm archivally permanent silver halide film produced to internationally accepted standards in the NMA 98-image format

Microfiches produced by Micromedia, Bicester, Oxon